Science of Sintering, **52** (2020) 41-52

doi:https://doi.org/10.2298/SOS2001041M

UDK: 519.718; 620.181.4; 666.3.019; 661.112.3

Synthesis and Characterization of Monophase Cao-TiO_2-SiO_2 (Sphene) Based Glass-Ceramics

Jelena Maletaškić[1,5*)], Bratislav Todorović[2], Martina Gilić[3], Milena Marinović Cincović[4], Katsumi Yoshida[5], Anna Gubarevich[5], Branko Matović[1]

[1]Institute of Nuclear Sciences Vinča, Department of Material Science, Center of Exselence, CEXTREME LAB University of Belgrade, P. O. Box 522, 11000 Belgrade, Serbia

[2]Faculty of Technology, University of Niš, P.O. Box 79, 16000 Leskovac, Serbia

[3]Institute of Physics, University of Belgrade, Pregrevica 118, 11080 Belgrade, Serbia

[4]Institute of Nuclear Sciences Vinča, Laboratory for Radiation Chemistry and Physics, University of Belgrade, Mike Petrovića Alasa 12-14, P.O. Box 522, 11001 Belgrade, Serbia

[5]Laboratory for Advanced Nuclear Energy, Institute of Inovative Research, Tokyo Institute of Technology, 2-12-1, Ookayama, Meguro-ku, Tokyo, 152-8550 Japan

Abstract:

Sphene based glass-ceramics ($CaTiSiO_5$), an excellent candidate for a host lattice of ceramic materials and for nuclear waste immobilization, has been prepared from a powder mixture of $CaCO_3$, TiO_2 and SiO_2 using vibro-milling for homogenization. Starting powders were melted at 1400 °C for 2 h, cooled to room temperature, grounded again, then crystallized by thermal treatment yielding a sphene glass-ceramic. The evolution of the phase composition during thermal treatment was investigated by X-ray powder diffraction (XRPD), FT-IR, Raman and thermal analyses (TG-DTA). Pure synthetic single phase sphene was formed at 800 °C for 4 h, even it is very hard to obtain monophase powder at such low temperature. Powder morphology was analyzed by scanning electron microscopy (SEM).

***Keywords**: Sphene; Glass-ceramics; Mechanochemistry; XRPD, TG-DTA.*

1. Introduction

Glass-ceramics can be used for various applications, such as thermal, chemical, biological and dielectric ones. These kinds of materials offer great possibilities as we can control their properties, including strength, resistance to abrasion and coefficient of thermal expansion [1]. Another advantage is the simple fabrication process in combination with a lower production cost [2-5]. The synthesis of the parent glass is an important step in preparing the final glass-ceramic material because the precursors and their percentage in the glass composition manage the precipitation of the crystalline phases. The results of this process can provide glass-ceramic with the desired properties.

Beside the biomaterials field, the glass-ceramics can be used as nuclear waste storage. They are significantly more durable than borosilicate glasses in a wide variety of leachates at

*) **Corresponding author:** jelena.pantic@vinca.rs

neutral or alkaline pH values [6]. In previous research, the Canadian Nuclear Fuel Waste Management program has considered the possibility of waste storage with glass-ceramics containing crystalline titanite embedded in an aluminosilicate glass [7, 8]. It can also be used for the stabilization of waste sludge [9, 10] and other waste material [11, 12].

Sphene or titanite ($CaTiSiO_5$ or $CaTiO(SiO_4)$) belongs to the nesosilicate family of minerals. It crystallizes in monoclinic symmetry in two space groups: $A2/a$ and $P2_1/a$ [13]. Sphene is a phase well known for its excellent containment capacity and long-term behavior (high chemical durability and self-radiation resistance). It has good thermal stability and it is an excellent candidate as a host material [14], as well as biomedical engineering (coatings on Ti-6Al-4V) [15]. Furthermore, it can be used for nuclear waste disposal [16], luminescent materials [17] and pigments [18-21] because of the ability to incorporate many elements into its crystal lattice.

In our work, we report the synthesis of sphene without additional phases. It is very difficult to obtain pure synthetic monophase titanite, especially bellow 1200 °C. Several different methods like sol-gel, coprecipitation, combustion, spray pyrolysis, freeze-drying and hydrothermal methods have been used. In most cases, pure sphene was not obtained [22-27]. There are always some traces of crystobalite (SiO_2), perovskite ($CaTiO_3$), wollastonite ($CaSiO_3$) and other phases, besides sphene.

When preparing the glass-ceramics at the laboratory, the crystallization of the parent glass is carried in two-phase via thermal treatment: nucleation and growth. In this paper we present the evolution of the crystallization, followed by scanning electron microscopy (SEM), Fourier transforms infrared spectroscopy (FTIR), Raman spectroscopy and X-ray powder diffraction (XRPD), with the temperature of the crystal growth thermal treatment, in the range 650-1250 °C. The formation process from glass to the final glass-ceramic product is discussed for different temperature treatments.

2. Materials and Experimental Procedures

2.1. Powder preparation and synthesis

Reactants used in the synthesis were commercial powders: TiO_2 (Lab. Art. 808 E. Merck), SiO_2 (ASP-K-amorphous, Prahovo) and $CaCO_3$ (pro analysi, 11490, Kemika, Zagreb). Sample was prepared from stoichiometric amounts of powders and weighed 5 grams. The powder mixtures were homogenized in the vibratory mill (Fritsch Puloerisette Analysette Laborette, type 09 003, no. 155, 380 volt). Detailed description of the synthesis procedures for sample can be found in the original paper [28]. Samples were ground for 30 min in air atmosphere prior to melting at 1400 °C in a platinum crucible for 2 h. After melting, sample was poured in water and grinded for glass homogenization before further thermal treatment. The glass was transformed into glass-ceramics by annealing in an open-air atmosphere in furnace. Calcination of powders was carried out at different temperatures from 600 to 1250 °C in at a heating rate of 10 °C/min and a soaking period of 4 h in alumina crucibles.

2.2. Characterization

The thermal stability of samples was investigated by non-isothermal thermo-gravimetric analysis (TG) and DTA analysis using a SETARAM SETSYS Evolution-1750 instrument. The measurements were conducted at a heating rate of 10°C /min in a dynamic air atmosphere (flow rate 16 cm3/min) in the temperature range from 30 to 1250 °C

Fourier transform infrared spectroscopy (FTIR) was performed in the absorbance mode using a BOMEM Michelson Series MB FTIR spectrometer set to give undeformed spectra. The resolution was 4 cm^{-1} in the 400–2000 cm^{-1} analyzed range. The spectra were

obtained at room temperature from KBr pressed pellets prepared by mixing 1.5 mg of a sample with 150 mg of KBr.

All of the samples were characterized at room temperature by X-ray powder diffraction (XRPD) using Ultima IV Rigaku diffractometer equipped with Cu $K_{\alpha 1,2}$ radiation using a generator voltage (40.0 kV) and a generator current (40.0 mA). The range of 10 - 90 °2θ was used for all powders in a continuous scan mode with a scanning step size of 0.02 ° and at a scan rate of 2 °/min. Phase analysis was done by using the PDXL2 software (version 2.0.3.0) [23], with reference to the patterns of the International Centre for Diffraction Data database (ICDD) [29], version 2012.

The average crystallite size (*D*) was calculated on the basis of the full-width at half-maximum intensity (FWHM) of the main reflections by applying Scherrer's formula:

$$D_{hkl} = K\lambda / (\beta \cdot \cos\theta) \qquad (2)$$

where *K* is a Scherrer's constant (~0.9), λ is the wavelengths of the X-ray used, θ is diffraction angle and β is corrected half-width for instrumental broadening given as $\beta = (\beta_m - \beta_s)$ where β_m and β_s are observed half-width and half-width of the standard monoclinic sphene sample, respectively.

Internal lattice strain ($\Delta d/d$) of calcined samples was estimated from the Williamson–Hall plots, using following equation [30]:

$$\beta_{total} \cos\theta = (K\lambda)/D + (4\Delta d/d) \cdot \qquad (3)$$

where β_{total} represents full-width half-maximum of the characteristic XRPD peak and Δd is the difference of the d spacing corresponding to a typical peak. The strain of nanocrystals, $\Delta d/d$, can be estimated from the slope of function $\beta \cdot cos\theta$ vs. $sin\theta$ whereas crystallite size, *D*, can be estimated from the y-intercept.

Micro-Raman scattering measurements were performed at room temperature using a Jobin-Yvon T64000 triple spectrometer system equipped with a liquid-nitrogen cooled CCD detector. The λ=514.5 nm line of an Ar^+/Kr^+ mixed laser was used as an excitation source.

Microstructure and grain size were investigated using Field Emission Scanning Electron Microscopy (FESEM), performed on a JEOL-5200F Scanning electron microanalyzer.

3. Results and Discussion

The results of thermal analysis of sample (as- prepared glass) after melting at 1400 °C are presented in Figure 1. As TG curve indicates, there is no obvious mass loss. At low temperature (below 300 °C), small exotermic peaks corresponding to volatiles appear larger, presumable due to the use of coarse powder [31]. As shown in DTA curves, there is a small endothermic peak attributed to the glass transition temperature range. Its minimum that starts at 760 °C refers to the glass transition temperature (T_g). The temperature at 886 °C belongs to sharp exothermic peak, due to the amorphous-crystalline transformation. The maximum temperature belongs to the crystallization peak temperature (T_p).

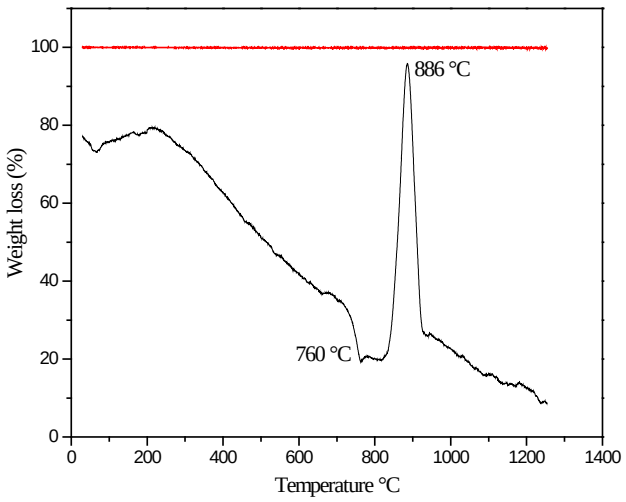

Fig. 1. DTA/TG diagram for as-synthesized amorphous glass up to a heat treatment temperature of 1250 °C. Black line – DTA; red line – TG.

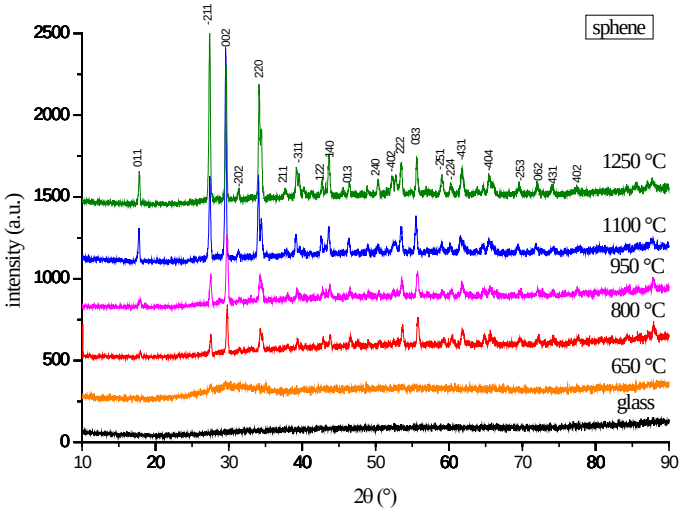

Fig. 2. X-ray powder diffraction patterns of sphene glass-ceramics (30 min grinding) after melting at 1400 °C and calcination at different temperatures (650-1250 °C). All the peaks belong to sphene.

The changes in the X-ray pattern due to annealing are presented in Figure 2. The pattern of glass sample and sample obtained at 650 °C corresponds to amorphous materials; no crystalline phases were detected. According to the results of TG/DTA, the glass starts to crystallize around 760 ºC. At 800 ºC X-ray powder diffraction results indicated that there was a significant change in the sample, and glass recrystallized to form sphene ($CaTiSiO_5$). All of the diffraction peaks belonging to sphene were observed. On further increasing the temperature up to 1250 °C, the intensity of sphene reflections increased, due to better crystallization. In addition, the peaks moved to slightly higher scattering angles on annealing, while the lattice volume decreases [32, 33]. The height of the strongest peak, the (200) reflection, is plotted against the annealing temperature in Figure 3, and the changes in lattice volume are similarly plotted in Figure 4. Sphene is a principle crystalline phase above 800 °C.

The main reflections in these patterns are observed at 2θ of 17, 27, 29, and 34 °, which are typical for the sphene structure. All the structure information was taken from American Mineralogist Crystal Data Structure Base (AMCDSB) [34]. Pure synthetic single phase sphene was formed at 800 °C for 4 h, even it is very hard to obtain monophase powder at such low temperature.

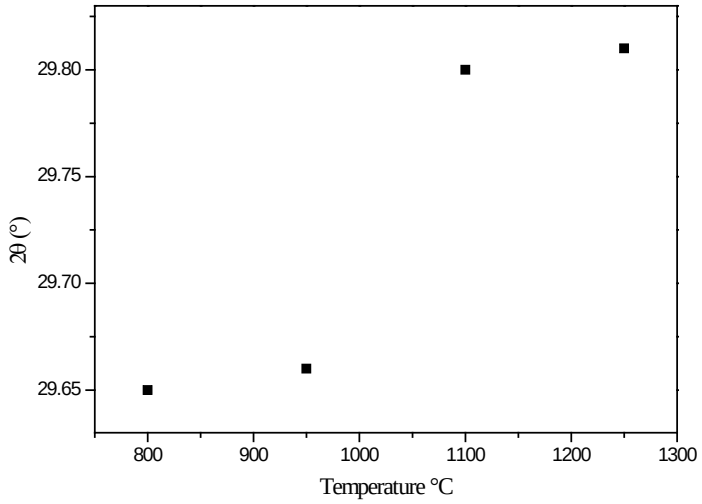

Fig. 3. Position of (200) X-ray powder diffraction peak, measured from samples calcinated at different temperatures (800-1250 °C).

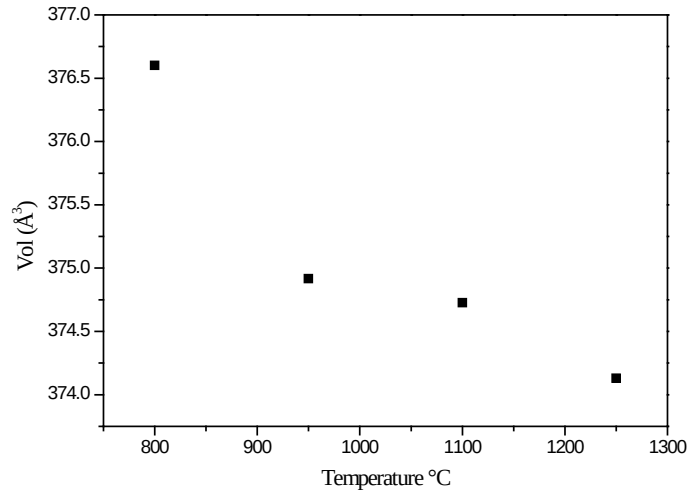

Fig. 4. Decrease in lattice volume as a function of annealing temperature. Measurements were made with samples calcinated at different temperatures (800-1250 °C).

The values of crystallite size and internal strain of samples after melting at 1400 °C and calcined at different temperatures for 4 h are presented in Table I. The average crystallite size increases with an increase in calcination temperature (up to 1100 °C) because of accelerated diffusion at higher temperatures, with decreasing the lattice parameters. At 1250 °C, due to close temperature range of melting point, crystallite size starts to decrease. Furthermore, the internal strain of samples calcined at different temperature which was

estimated from the slope of Williamson – Hall plots is presented in Figure 5. Just after the crystalization, there is no evident strain.

Tab. I Lattice parameter and crystallite size of sphene glass-ceramics (30 min grinding) after melting at 1400 °C and calcination at different temperatures (650-1250 °C).

Temperatures (°C)	Lattice parameter (Å)	β (°)	D (nm)
650	amorhous	/	/
800	a = 7.0859 b = 8.8062 c = 6.5478	112.8200	23
950	a = 7.0808 b= 8.7882 c = 6.5413	112.9181	25
1100	a = 7.0911 b = 8.7893 c = 6.5316	112.9995	28
1250	a = 7.0946 b = 8.7716 c = 6.5328	113.0340	16

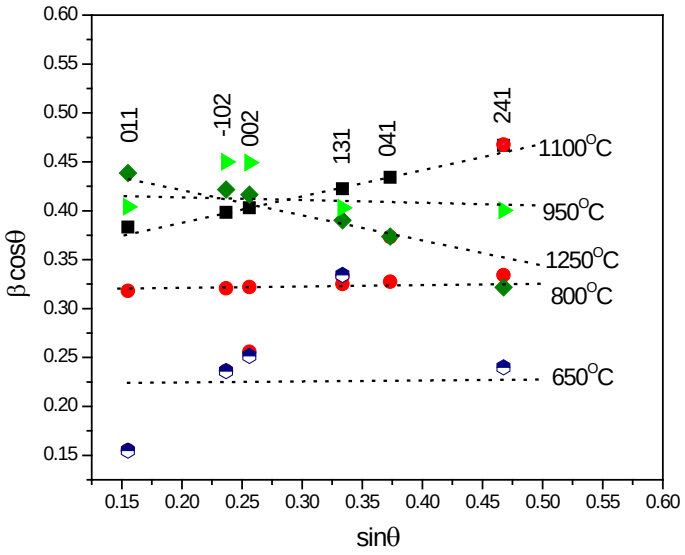

Fig. 5. Williamson-Hall plot of sphene glass-ceramics (30 min grinding) after melting at 1400 °C and calcination at different temperatures (650-1250 °C). The dotted lines are visual guides.

To confirm X-ray powder diffraction results, FT-IR measurements were done. FT-IR spectra of samples sintered at different temperatures are shown in Figure 6. From 800 °C up to 1250 °C, vibrations centered at about: 895 cm^{-1}, 870 cm^{-1}, 694 cm^{-1}, 561 cm^{-1}, 468 cm^{-1} and 424 cm^{-1} correspond to vibration of sphene and they are in good agreement with published data [35-38]. The spectra are dominated by the IR band near 870 cm^{-1} which is attributed mainly to SiO_4 stretching modes. The broad band near 694 cm^{-1} is associated with TiO_6 octahedral stretching modes, polarized along the crystallographic *a*-axis and it is related to the crystal quality [39]. Vibration band around 1636 cm^{-1} due to the asymmetric stretching mode of CO_3^{-2} were also detected [40].

The effect of temperature increase is seen as a decrease in band width, an increase in band intensity associated with Si-O bending at 561 cm^{-1} and the Si-O stretching band at about 870 cm^{-1} [41, 42]. All peaks shift to higher wavenumbers with increasing temperature.

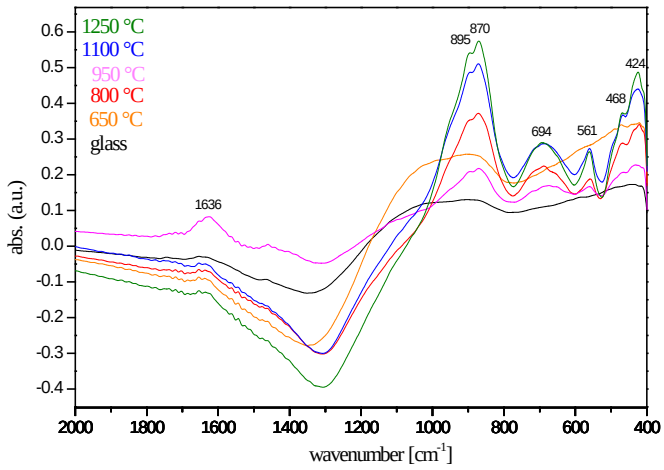

Fig. 6. FTIR absorption spectra of sphene glass-ceramics after (30 min grinding) after melting at 1400 °C and calcination at different temperatures (650-1250 °C).

The Raman spectra collected from samples are shown in Figure 7. The characteristic bands of sphene that occur in Raman spectra are centered around 167, 258, 473, 548 and 608 cm^{-1} [38, 43]. All peaks shift to higher wavenumbers with increasing temperature.

The position of the peak near 608 cm^{-1} belongs to a symmetrical mode from Ti–O bond stretching and Ti–O–Ti bond bending [44-46]. As peak intensity increases with increasing temperature, band width of this peak decreases [47].

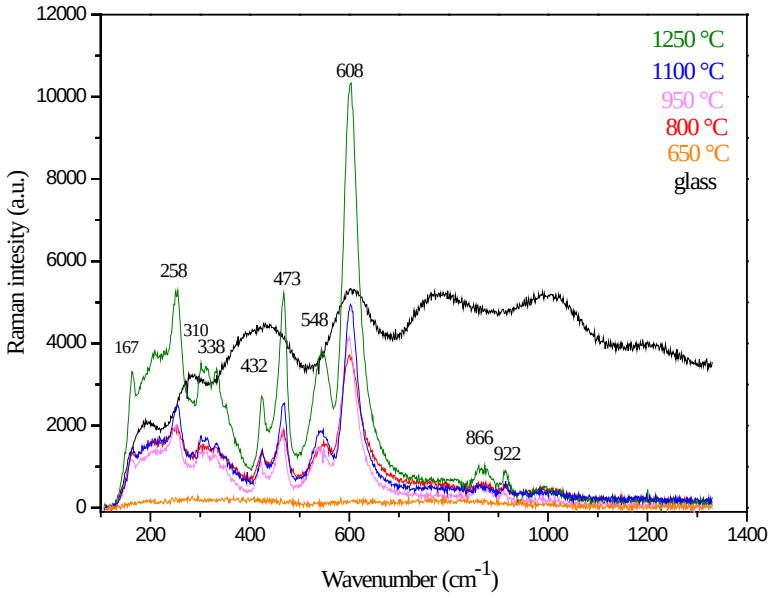

Fig. 7. The Raman spectra of sphene glass-ceramics (30 min grinding) after melting at 1400 °C and calcination at different temperatures (650-1250 °C).

On increasing temperature, the peaks near 432 and 473 cm^{-1} related to SiO_4 bending modes as well as the external SiO_4 mode near 258 cm^{-1} have the same dependence, an increasing wavenumber and a decreasing band width. Peak near 473 cm^{-1} belongs to the SiO_4 bending mode [43]. The Raman peaks near 866 cm^{-1} correspond to Si-O stretching modes in orthosilicates [47].

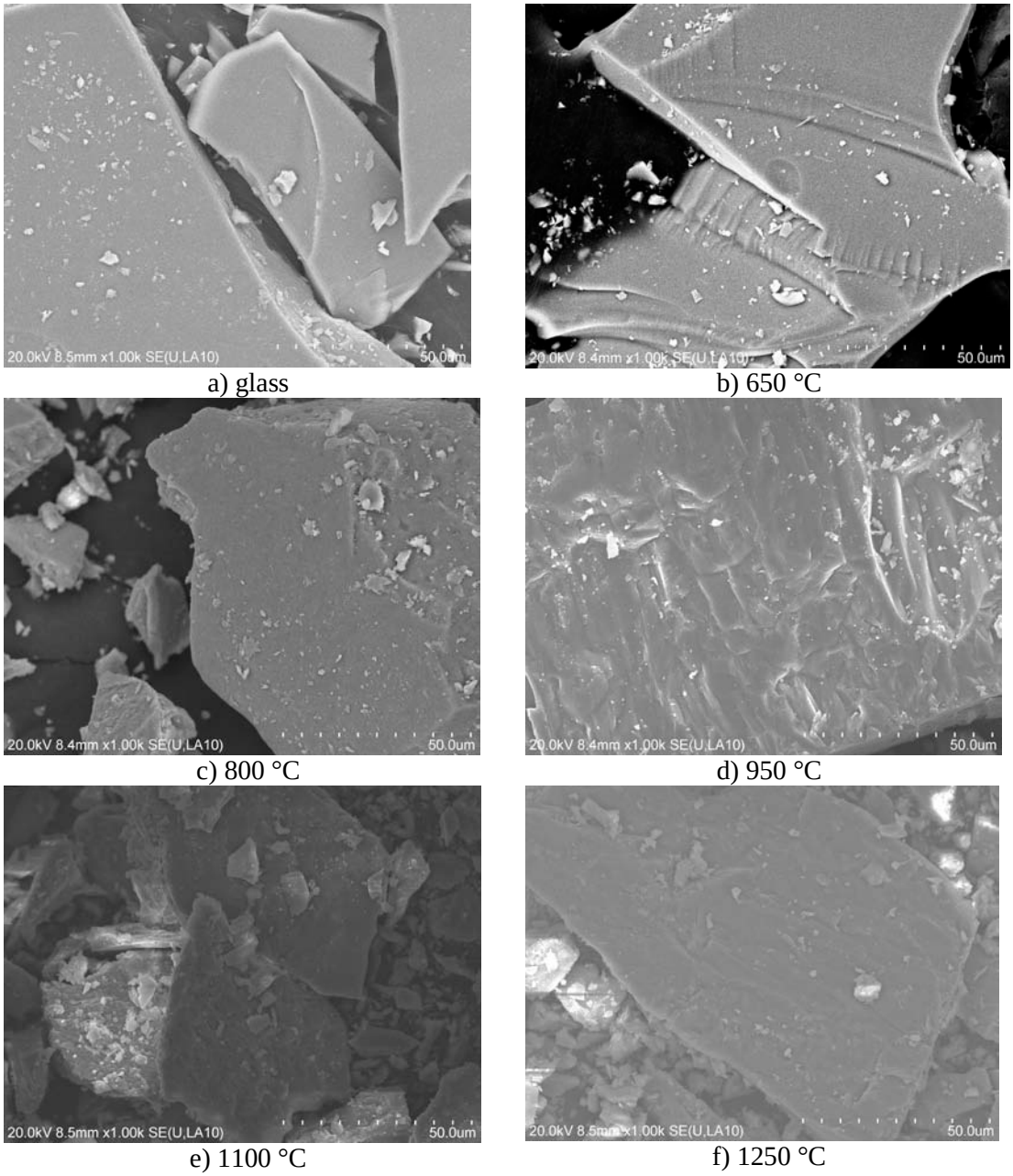

a) glass b) 650 °C

c) 800 °C d) 950 °C

e) 1100 °C f) 1250 °C

Fig. 8. SEM micrographs (a-f) of sphene glass-ceramics (30 min grinding) after melting at 1400 °C and calcination at different temperatures (650-1250 °C).

Due to the increasing degree of cristalization all peaks shift to higher wavenumbers. Ti-O bond stretching band shifts from 601 ± 0.5 cm^{-1} to 608 ± 0.5 cm^{-1}. O-Si-O bending modes at 466 ± 0.5 cm^{-1} shifts to 473 ± 0.5 cm^{-1}, 422 ± 0.5 cm^{-1} shifts to 432 ± 0.5 cm^{-1} and 253± 0.5 cm^{-1} shifts to 258 ± 0.5 cm^{-1}. Si-O stretching modes at 862 ± 0.8 cm^{-1} shifts to a

position at 866 ± 0.8 cm^{-1} (Figure 7). The lowest-energy mode occurring near 167 cm^{-1} also shows a slight shift to higher wavenumbers, from 161 ± 0.5 cm^{-1} shift to 167 ± 0.5 cm^{-1}.

Regarding amorphous systems, in Ti–Si–O frameworks the Ti^{4+} cations can occur as 6–, 5– and 4– coordinated [48, 49], and penta– and tetra–coordinated Ti^{4+} can be found in heavily metamict sphene [50-52]. When decreasing Ti coordination, the Ti–O bond strength increases. As a result, in a disordered framework, the Ti–O bond stretching mode would move to higher wavenumbers as compared to the Ti–O bond stretching mode having only TiO_6 octahedra.

The SEM micrographs of glass-ceramics obtained at various temperatures are shown in Figure 8. Samples were crushed in mortal prior the measurents. For glass obtained at 650 °C, particles with irregular shapes were observed, as shown in Figure 6(b). After being calcined at higher temperatures (800-1250 °C), similar anhedral shape is seen (Figure 8 (c–f)). Particles have a smooth fracture surface with no obvious cracks or faults on the surface.

4. Conclusion

Glass and glass-ceramics in the $CaO–TiO_2–SiO_2$ system have been successfully synthesized. From DTA curves, glass transition temperature (T_g) starts at 760 °C and temperature at 886 °C belongs to the crystallization peak temperature (T_p). X-ray powder diffraction results indicated that at 800 ℃ glass recrystallize to form sphene ($CaTiSiO_5$), and the peaks moved to slightly higher scattering angles on annealing, while the lattice volume decreases. Pure synthetic single phase sphene was formed at 800 °C for 4 h, despite being difficult to obtain monophase powder at such low temperature. The effect of temperature increase in FT-IR and Raman measurements is seen as a decrease in band width and an increase in band intensity. All peaks shift to higher wavenumbers with increasing temperature, according to the Raman. SEM images showed anhedral shaped particles.

For crystal growth temperature (T_c) ranging from 800 to 1250 °C, sphene is the only crystalline phase. Thus there is a wide range of temperature for the preparation of monophase sphene-based glass-ceramics that can be designed as durable waste forms for immobilization.

Acknowledgments

Financial support from the Serbian Education and Science Ministry in the Framework of project No. 45012 is gratefully acknowledged. One of the authors Jelena Maletaskic, as well as Branko Matovic, gratefully acknowledge the financial support from the Tokyo Institute of Technology, Laboratory for Advanced Nuclear Energy, Institute of Innovative Research, 2-12-1, O-okayama, Meguro-ku, Tokyo 152-8550, as visiting professors.

5. References

1. D.U. Tulyaganov, S. Agathopoulos, J.M. Ventura, M.A. Karakassides, O. Fabrichnaya, J.M.F. Ferreira, Synthesis of glass–ceramics in the $CaO-MgO-SiO_2$ system with B_2O_3, P_2O_5, Na_2O and CaF_2 additives, J. Eur. Ceram. Soc. 26 (2006) 1463-1471.
2. W. Holand, G. Beall, Glass–Ceramic Technology, 2nd ed. Wiley-American Ceramic Society, Westerville, OH, 2012.
3. N.M. Pavlushkin, Principals of Glass Ceramics Technology, 2nd ed. Stroiizdat, Moscow, 1979 (in Russian).
4. P.W. McMillan, Glass-Ceramics. Academic Press, London, 1964.
5. Z. Strnad, Glass-Ceramic Materials. Elsevier, Amsterdam, 1986.

6. P.J. Hayward, D.C. Doern, I.M. George, Dissolution of a sphene glass- ceramic, and of its component sphene and glass phases in Ca-Na-Cl brines, J. Am. Ceram. Soc. 73 (1990) 544-511.
7. P.J. Hayward, Glass ceramics. In W. Lutze and R. Ewing, Eds., Radioactive waste forms for the future, Elsevier, New York (1988) 427-492.
8. P. Hayward, E. Cechetto, Development of sphene-based glass ceramics tailored for Canadian waste disposal conditions, In Topp, S., Ed., Scientific Basis for Nuclear Waste Management 3 (1982) 91-98.
9. I. Krstić, S. Zec, V. Lazarević, M. Stanisavljević, T. Golubović, Use of Sintering to Immobilize Toxic Metals Present in Galvanic Sludge into a Stabile Glass-Ceramic Structure, Sci. Sinter. 50 (2018) 139-147.
10. A. P. Parra, M. Vlasova, P. A. Márquez Aguilar, T. Tomila, Peculiarities of a Glass-Sludge Mixture Subjected to Low-Temperature Treatment Sci. Sinter. 49 (2017) 207-224.
11. M. Cocic, B. Matovic, M. Posarac, T. Volkov-Husovic, J. Majstorovic, V. Tasic, S. Devic, N. Vusovic, Thermal Shock Properties of Glass-ceramics Synthesized From a Glass Frit, Sci. Sinter. 49 (2017) 139-147.
12. M. Cocić, M. Logar, S. Erić, V. Tasić, S. Dević, S. Cocić, B. Matović, Application of the Final Flotation Waste for Obtaining the Glass-ceramic Materials, Sci. Sinter. 49 (2017) 431-443.
13. E.S. Dana, Manual of mineralogy. 17th ed. John Wiley & Sons Inc. (1959) 412-413.
14. M. Gascoune, Evidence for the stability of the potential nuclear waste host, sphene, over geological time, from uranium-lead ages and uranium series measurement. App. Geolchem. 1 (1986) 199-210.
15. C. Wu, Y. Ramaswamy, X. Liu, G. Wang, H. Zreiqat, Plasma-sprayed $CaTiSiO_5$ ceramic coating on Ti-6Al-4V with excellent bonding strength, stability and cellular bioactivity, J. R. Soc. Interface 6 (2009) 159-168.
16. A.E. Ringwood, S.E. Kesson, K.D. Reeve, D.M. Levins, E.J. Ramm, SYNROC. In: Lutze W, Ewing RC, editors. Radioactive waste forms for the future, North-Holland, Amsterdam (1988) 233-334.
17. M. Gaft, L. Nagli, R. Reisfeld, G. Panczer, Laser-induced time-resolved luminescence of natural titanite $CaTiOSiO_4$, Opt. Mater. 24 (2003) 231-241.
18. P. Escribano, C. Guillem, J. Alarcon, Cr-SnO_2-CaO-SiO_2 based ceramic pigments, Am. Ceram. Soc. Bull. 63 (1984) 1492-1494.
19. J. Carda, P. Escribano, G. Monros, M.D. Rodrigo, J. Alarcon, Co-SnO_2-CaO-SiO_2 based ceramic pigments, Interceram. 39 (1990) 22-24.
20. L. Ferrer, M. Sales, J. Alarcon, Sphene structure based ceramic pigments, Third Euro-ceram. 2 (1993) 935-939.
21. J. Pantić, M. Prekajski, M. Dramićanin, N. Abazović, N. Vuković, A. Kremenović, B. Matović, Preparation and characterization of chrome doped sphene pigments prepared via precursor mechanochemical activation, J. Alloy. Comp. 579 (2013) 290-294.
22. T.S. Lyubenova, F. Matteucci, A. Costa, M. Dondi, J. Carda. Ceramic pigments with sphene structure obtained by both spray- and freeze drying techniques, Powder Technol. 193 (2009) 1-5.
23. T.S. Lyubenova, F. Matteucci, A.L. Costa, M. Dondi, M. Ocaña, J. Carda, Synthesis of Cr-doped $CaTiSiO_5$ ceramic pigments by spray drying, Mater. Res. Bull. 44 (2009) 918-924.
24. T. Malcherek, C.M. Domeneghetti, V. Tazzoli, E.K.H. Salje, U. Bismayer, A high temperature diffraction study of synthetic titanite $CaTiOSiO_4$, Phase Transitions 69 (1999) 119-131.
25. M. Muthuraman, N.A. Dhas, K.C. Patil, Combustion synthesis of oxide materials for nuclear waste immobilization, Bull. Mater. Sci. 17 (1994) 977-987.

26. M. Muthuraman, K.C. Patil, Synthesis, properties, sintering and microstructure of sphene, $CaTiO_5$: A comparative study of coprecipitation, sol-gel and combustion processes, Mater. Res. Bull. 33 (1998) 655-661.
27. R. Ellemann-Olesen, A high-temperature diffraction study of the solid solution $CaTiOSiO_4$-$CaTiOGeO_4$, Am. Miner. 90 (2005) 1325-1334
28. J. Pantić, A. Kremenović, A. Došen, M. Prekajski, N. Stanković, Z. Baščarević, B. Matović, Influence of mechanical activation on sphene based ceramic material synthesis, Ceram. Inter. 39 (2013) 483-488.
29. PDXL Version 2.0.3.0 Integrated X-ray Powder Diffraction Software. Tokyo, Japan: Rigaku Corporation (2011) 196-8666.
30. Powder Diffraction File, PDF-2 Database and announcement of new database release 2012, International Centre for Diffraction Data (ICDD).
31. J. Rodriguez-Carvajal, Collected Abstract of Powder Diffraction Meeting, Toulouse (1990) 127.
32. J.B. Higgins, P.H. Ribbe, The crystal chemistry and space groups of natural and synthetic titanites, Am. Mineral. 61 (1976) 878-888.
33. E.R. Vance and J.B. Metson, Radiation damage in natural titanite, Phys. Chem. Minerals 12 (1985) 255-260
34. R.T. Downs, M. Hall-Wallace, The American Mineralogist Crystal Structure Database, Am. Min. 88 (2003) 247-250.
35. J.A. Gadsden, Infrared Spectra of minerals and related inorganic compounds, Butterworth, Group adresses, England, Australia, Canada, New Zealand, South Africa, U.S.A., 1975.
36. H. Moenke, Mineralspectren. Deutsche Akademie der Wissenschaften zu Berlin, Akademie – Verlag – Berlin, 1962.
37. J. Pantić, V. Kahlenberg, V. Poharc-Logar, A. Kremenović, Natural CaO-TiO_2-SiO_2 based ceramics, Process. Appl. Ceram. 5 [2] (2011) 79-84.
38. J. Pantic, V. Urbanovich, V. Poharc- Logar, B. Jokić, M. Stojmenović, A.Kremenović, B. Matović, Synthesis and characterization of high-pressure and high-temperature sphene ($CaTiSiO_5$), Phys. Chem. Miner. 41 (2014) 775-782.
39. H.W. Meyer, M. Zhang, U. Bismayer, E.K.H. Salje, C. Schmidt, S. Kek, W. Morgenroth, T. Bleser, Phase transformation of natural titanite: An infrared, Raman spectroscopic, optical birefringence and X-ray diffraction study. Phase Trans. 59 (1996) 39-60.
40. P.J. Hayward, E.R. Vance, C.D. Cann, S.L. Mitchell Crystallization of sphene-based glass-ceramics for immobilization of high-level nuclear fuel reprocessing wastes. In: Wicks GG, Ross WA (eds) Advances in Ceramics. Am Ceramic Society, (1984c) 291-301.
41. E.K.H. Salje, U. Bismayer, Hard Mode Spectroscopy: The Concept and Applications, Phase Trans. 63 (1997) 1-75
42. M. Zhang, E.K.H. Salje, U. Bismayer, Structural phase transition near 825 K in titanite: Evidence from infrared spectroscopic observations, Am. Mineral. 82 (1997) 30-35.
43. A.M. Heyns, P.M. Harden, L.C. Prinsloo, Resonance Raman study of the high-pressure phase transition in chromium-doped titanite, $CaTiOSiO_4$, J. Raman Spectrosc. 31 (2000) 837-841.
44. V. Kostov-Kytin, B. Mihailova, Y. Kalvachev, M. Tarassov, Atomic arrangements in amorphous sodium titanosilicate precursor powders, Micropor. Mesopor. Mater. 86 (2005) 223-230.
45. Y. Su, M.L. Balmer, B.C. Bunker, Raman Spectroscopic Studies of Silicotitanates, J. Phys. Chem. B. 104 (2000) 8160-8169
46. T. Beirau, B. Mihailova, G. Matveeva, U. Kolb, T. Malcherek, L.A. Groat, U. Bismayer Structural anisotropy and annealing-induced nanoscale atomic rearrangements in metamict titanite, Am. Mineral. 97 (2012) 1354-1365.

47. E. Dowty, Vibrational interactions of tetrahedra in silicate glasses and crystals: I. Calculations on ideal silicate-aluminate-germanate structural units, Phys. Chem. Mineral. 14 (1987) 80-93.
48. H.V. Alberto, N.A. de Campos, B.O. Mysen, The structural role of titanium in silicate glasses - a Raman-study of the system $CaO-SiO_2-TiO_2$. Phys. Chem. Glasses 36 (1995) 114-122.
49. H. Nasu, K. Kurachi, A. Mito, J. Matsuoka, K. Kamiya, Second harmonic generation and structure of mixed alkali titanosilicate glasses. J. Non-Cryst. Solids 217 (1997) 182-188.
50. F.C. Hawthorne, L.A. Groat, M. Raudsepp, N.A. Ball, M. Kimata, F.D. Spike, R. Gaba, N.M. Halden, G.R. Lumpkin, R.C. Ewing, R.B. Greegor, F.W. Lytle, T.S. Ercit, G.R. Rossman, F.J. Wicks, R.A. Ramik, B.L. Sherriff, M.E. Fleet, C. McCammon, Alpha-decay damage in titanite, Am. Mineral. 76 (1991) 370-396.
51. F. Farges, Fivefold-coordinated Ti^{4+} in metamict zirconolite and titanite: A new occurrence shown by Ti K-edge XANES spectroscopy, Am. Mineral. 82 (1997) 44–50.
52. M. Zhang, E.K.H. Salje, U. Bismayer, L.A. Groat, T. Malcherek, Metamictization and recrystallization of titanite: An infrared spectroscopic study. Am. Mineral. 87 (2002) 882-890.

Сажетак: *Стакло-керамика на бази сфена ($CaTiSiO_5$), као одличан кандидат за имобилизацију нуклеарног отпада, припремљена је из смеше реактаната TiO_2, SiO_2 и $CaCO_3$ користећи вибро-млин за хомогенизацију. Почетни прахови су стопљени на 1400 °C током 2h, охлађени до собне температуре, поново самлевени, затим калцинисани на одређеним температурама дајући стакло-керамику. Еволуција фазног састава током калцинације испитивана је рендгенском дифрактометријом праха, ИЦ спектроскопијом, Раманском и термалном анализом (ТГ-ДТА). Сфен, без додатних фаза, формиран је на 800 °C током 4h, иако га је веома тешко добити у монофаном облику на тако ниској температури. Морфологија прахова је анализирана скенирајућом електронском микроскопијом (СЕМ).*

Кључне речи*: сфен стакло-керамика, механохемија, рендгенска дифрактометрија праха, ТГ-ДТА.*